# A Generalized Fault Location Approach for Any Type of Power Network

**Cesar Galvez** * **Ali Abur** **

\* Northeastern University, Boston, MA 02125 USA (e-mail: galveznunez.c@northeastern.edu).
\*\* Northeastern University, Boston, MA 02125 USA (e-mail: a.abur@northeastern.edu).

**Abstract:** This paper presents a generalized fault location algorithm that can locate faults for any type of power network configuration. It enhances previous work presented by the authors by reducing the estimation steps but keeping its robustness and redundancy against traveling wave attenuation by power transformers, bad data, voltage signal errors and the impact of Inverter Based Power Sources (IBPSs). This is accomplished by forming arrays containing the network parameters and time-of-arrivals (ToAs) for fault signals captured by Digital Fault Recorders (DFRs), which are used as inputs to the algorithm to compute the accurate fault localization. The IEEE 39-bus system is used to validate the algorithm under different fault conditions using Electromagnetic Transients Program and Matlab as simulation tools.

*Keywords:* Fault Location, DFR Optimal Placement, electromagnetic transients, wavelet transform, traveling waves .

## 1 Introduction

High penetration of Inverter-Based Power Sources (IBPSs) such as photovoltaic parks, wind parks, and battery energy storage systems (BESS) into the power network presents new challenges due to its significant impact on the transient behaviour of power systems. IBPSs' integration also changed the traditional configuration of power grids by facilitating bidirectional power flows, often injecting reverse power to neighboring systems in the grid. While the bidirectionally of power flows introduces redundancy of power supply, it also creates new challenges in terms of operation, protection, fault location and detection. Reverse power flows drastically impacts existing protection coordination schemes and increases probability of faults in power grids. Hence, a fast and robust fault location method that can be used for any network configuration using a minimum number of Digital Fault Recorders (DFRs) is badly needed.

Fault location methods can be classified into three categories: impedance-based, (Sachdev and Agarwal (1988)), artificial intelligence(AI) Yadav and Swetapadma (2015), and traveling wave (TW) methods (Galvez and Abur (2022)). AI algorithms are mostly used in the fault classification and faulted section identification Yadav and Swetapadma (2015), but present limitations for estimating the precise fault location. The impedance-based methods are vulnerable to unknown fault resistances Filomena et al. (2008), unbalanced loads, non-transposed lines and the presence of IBPSs Paladhi and Pradhan (2020). Traveling wave (TW) methods are accurate and remain robust under the above presented limitations. Recent technology developments enables sampling rates of 1 MHz by digital fault recorders (DFRs) SEL ((accessed 2022) and the integrated optical sensors for voltage measurement Ding et al. (2018).

The work presented in this paper enhances the methods proposed earlier by the authors Galvez and Abur (2020); Galvez and Abur (2022). The first does not fully exploit redundancy in fault distance estimation and it is primarily deigned for radial networks. The second method eliminates the need to first identify the faulted section, and involves two stages.

In this paper, a generalized robust fault location algorithm that can locate faults in any distribution or transmission network will be presented. The method first models the network as a weighted un-directed graph and uses the Optimal DFR Placement (ODP) to place a small number of DFRs in the network. The shortest travel times formed by DFR pairs and time of arrivals (ToAs) captured by DFRs are put into arrays and used as entries into the fault location algorithm. The algorithm does not need to first identify the faulted section. Instead, it forms and uses arrays as inputs to a generalized fault location algorithm which works accurately and reliably on power grids of any configuration.

## 2 Problem Formulation

Fault location problem is considered in two stages. The first stage aims to place an optimal set of DFRs in order to facilitate fault location in the given system. The second stage involves the computational algorithm that yields the accurate fault location based on the transient recordings of the placed DFRs. Both stages of the problem formulation will be described below via a small tutorial example.

Consider the small transmission system shown in Fig. 1. The system contains a synchronous generator, wind turbines, photovoltaic sources connected at buses 1, $n$ and $n-3$ respectively. The meshed network contains two circuit

breakers CB1 and CB2 that connect buses $n-2$ and $n-3$. Note that when the circuit breakers are open, the system will be configured as a strictly radial network, when they are closed, the network will become a meshed system. Consider the fault at F1 occurring along the underground cable shown in Fig. 1.
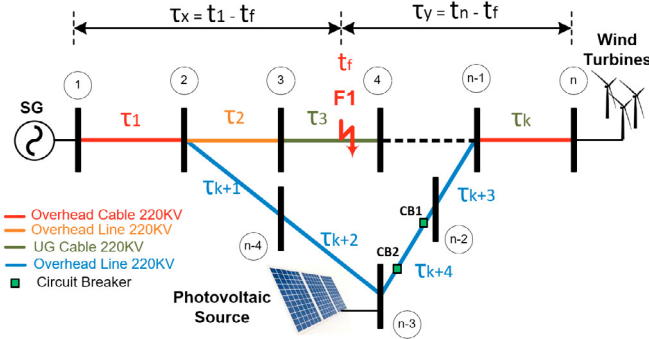


Fig. 1. Small Transmission System

First, the optimal DFR placement strategy will be described using the same small system example.

### 2.1 Optimal DFR Placement (ODP)

The small transmission system of Fig. 1 is first represented as a weighted un-directed graph denoted by $G = (\nu, \varepsilon, \omega)$, where $\nu$ is the set of buses or nodes with size $n$, $\varepsilon$ is the set of edges or lines with size $L$ in which $L \geq n-1$, and $\omega$ is the set of weights represented by two parameters $(\tau, \upsilon)$, where $\tau_i$ ($\mu s$) and $\upsilon_i$ ($km/s$) are the travel times and traveling wave speed at each edge $i$. The travel times $\tau_i$ ($\mu s$) are computed by $(\tau_i = l_i/\upsilon_i = l_i\sqrt{L_i.C_i})$, where $l_i$ is the line length, and $\upsilon_i$ is the wave speed for the edge $i$. Also, it can be computed using the conductor capacitance $C_i$ and inductance $L_i$ per unit length. Note that the speed of traveling waves in overhead lines is very close to the speed of light $3x10^5 km/s$. The Optimal DFR placement (ODP) Discrete Wavelet Transform (DWT) problem and its proposed solution will be described next for meshed and radial distribution networks respectively.
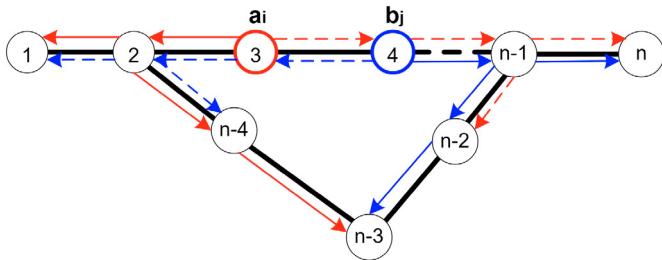


Fig. 2. Weighted Un-directed Graph of Meshed Transmission System

### 2.1.1 Optimal DFR Placement For Meshed Networks

Consider a weighted un-directed graph of the transmission system shown in Fig. 2. When a short-circuit occurs in a line-cable hybrid network, the fault-generated travel waves propagate from the short-circuit location to system buses following the shortest traveling time routes. Assume that the faulted edge is (3-4). The shortest traveling times from terminal buses 3 ($a_i$) and 4 ($b_j$) to all other buses

$n$ (red and blue arrows respectively) can be computed as shown in Fig. 2. Note that the shortest travel time paths using bus 3 as the reference must include its adjacent bus 4, whose shortest routes are represented by dashed red arrows in Fig. 2. Also, using bus 4 as the reference, the shortest travel time routes must include its adjacent bus 3, marked by dashed blue arrows in Fig. 2.Therefore, if a fault occurs along branch 3-4, the shortest travel times formed by dashed red and and blue arrows will be the only ones that can be used to compute the fault distance. Hence, a binary vector for each terminal bus of branch 4-3 can be determined as below.

$$
T_{(a_i,n)} = \begin{cases} 1 & \text{If there is at least a shortest travel} \\ & \text{time from bus "}a_i\text{" to system buses} \\ & \text{"}n\text{" containing bus "}b_j\text{"} \\ 0 & \text{Otherwise} \end{cases}
$$
(1)

$$
T_{(b_j,n)} = \begin{cases} 1 & \text{If there is at least a shortest travel} \\ & \text{time from bus "}b_j\text{" to system buses} \\ & \text{"}n\text{" containing bus "}a_i\text{"} \\ 0 & \text{Otherwise} \end{cases}
$$
(2)

where, $a_i$ and $b_j$ are the terminal buses of network branches and $n$ represents all other system buses. The binary vectors for buses 3 and 4 can then be formed as:

$$
T_{(a_3,n)} = a_3 \begin{bmatrix} 1 & 2 & 3 & 4 & ..... & n-3 & n-2 & n-1 & n \\ 0 & 0 & 0 & 1 & ..... & 0 & 1 & 1 & 1 \end{bmatrix}
$$

$$
T_{(b_4,n)} = b_4 \begin{bmatrix} 1 & 2 & 3 & 4 & ..... & n-3 & n-2 & n-1 & n \\ 1 & 1 & 1 & 0 & ..... & 0 & 0 & 0 & 0 \end{bmatrix}
$$

Using the procedure for all other system branches, the following $2L \times n$ binary matrix $T$ can be formed, where $L$ represents the number of branches in the system:

$$
T = \begin{matrix} & \begin{matrix} 1 & 2 & 3 & 4 & .... & n-3 & n-2 & n-1 & n \end{matrix} \\ \begin{matrix} a_1 \\ b_2 \\ a_2 \\ b_3 \\ a_3 \\ b_4 \\ . \\ . \\ . \\ a_{n-1} \\ b_n \end{matrix} & \begin{bmatrix} 0 & 1 & 1 & 1 & .... & 1 & 1 & 1 & 1 \\ 1 & 0 & 0 & 0 & .... & 0 & 0 & 0 & 0 \\ 0 & 0 & 1 & 1 & .... & 0 & 1 & 1 & 1 \\ 1 & 1 & 0 & 0 & .... & 1 & 0 & 0 & 0 \\ 0 & 0 & 0 & 1 & .... & 0 & 1 & 1 & 1 \\ 1 & 1 & 1 & 0 & .... & 0 & 0 & 0 & 0 \\ . & . & . & . & .... & . & . & . & . \\ . & . & . & . & .... & . & . & . & . \\ . & . & . & . & .... & . & . & . & . \\ 0 & 0 & 0 & 0 & .... & 0 & 0 & 0 & 1 \\ 1 & 1 & 1 & 1 & .... & 1 & 1 & 1 & 0 \end{bmatrix} \end{matrix}
$$
(3)

Having formed the matrix $T$, the ODP problem can be formulated for a system with $n$ buses and $L$ branches as follows:

$$
\text{minimize} \sum_{i=1}^{N} w_k \cdot x_k
$$
(4)

$$
s.t. \ [T][X] \geq b
$$
(5)

where,

$T = [\,T\,]_{2L \times n}$

$X = [\,x_1, \ x_2, \ x_3, ....., \ x_n\,]^T_{n \times 1}$

$$b = [1, \ 1, \ 1, .....,\ 1]^T_{2L \times 1}$$

$X_k$ will be 1 if a DFR is installed at bus $k$ or 0 otherwise, and $w_k$ represents the installation cost of $DFR_k$ at bus $k$. Assuming that the cost of installation for all the DFRs is the same, the optimal DFR placement (ODP) for the small transmission network of Fig. 1 will be given by:

$$X^T = \begin{array}{cccccccccc} & 1 & 2 & 3 & 4 & ..... & n-3 & n-2 & n-1 & n \\ & [\mathbf{1} & 0 & 0 & 0 & ..... & \mathbf{1} & 0 & 0 & \mathbf{1}] \end{array}$$

This implies that buses 1, $n-3$, and $n$ are optimal locations for installing DFRs.
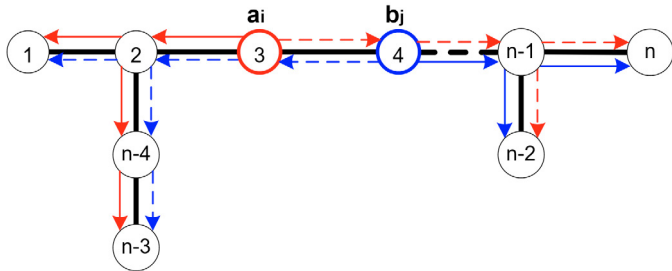


Fig. 3. Weighted Un-directed Graph of Radial Transmission System

#### 2.1.2 Optimal DFR Placement For Radial Networks

The same ODP strategy used for meshed networks will also be utilized for radial networks. Assume that the two circuit breakers CB1 and CB2 in Fig. 1 are open to transform the meshed system to a radial network. The radial network is then represented as a weighted un-directed graph as shown in Fig. 3. Now, select the faulted branch 3-4 from the radial network to compute the binary vector for each terminal bus of edge 3-4 using condition 1 and 2 as shown below.

$$T_{(a_3,n)} = a_3 \begin{array}{cccccccccc} & 1 & 2 & 3 & 4 & ..... & n-3 & n-2 & n-1 & n \\ & [0 & 0 & 0 & 1 & ..... & 0 & 1 & 1 & 1] \end{array}$$

$$T_{(b_4,n)} = b_4 \begin{array}{cccccccccc} & 1 & 2 & 3 & 4 & ..... & n-3 & n-2 & n-1 & n \\ & [1 & 1 & 1 & 0 & ..... & 1 & 0 & 0 & 0] \end{array}$$

Note that the binary vectors corresponding to the terminal buses of branch 3-4 are represented by dashed red and blue arrows in Fig. 3. Repeating the same procedure for all other network branches, the following $2L \times n$ binary matrix $T$ can be formed for the radial network, where $L$ is the number of branches, which will be reduced in size due to the disconnection of branch $(n-2)$ - $(n-3)$.

$$T = \begin{array}{c} \\ a_1 \\ b_2 \\ a_2 \\ b_3 \\ a_3 \\ b_4 \\ . \\ . \\ . \\ a_{n-1} \\ b_n \end{array} \begin{bmatrix} 1 & 2 & 3 & 4 & .... & n-3 & n-2 & n-1 & n \\ 0 & 1 & 1 & 1 & .... & 1 & 1 & 1 & 1 \\ 1 & 0 & 0 & 0 & .... & 0 & 0 & 0 & 0 \\ 0 & 0 & 1 & 1 & .... & 0 & 1 & 1 & 1 \\ 1 & 1 & 0 & 0 & .... & 1 & 0 & 0 & 0 \\ 0 & 0 & 0 & 1 & .... & 0 & 1 & 1 & 1 \\ 1 & 1 & 1 & 0 & .... & 1 & 0 & 0 & 0 \\ . & . & . & . & .... & . & . & . & . \\ . & . & . & . & .... & . & . & . & . \\ . & . & . & . & .... & . & . & . & . \\ 0 & 0 & 0 & 0 & .... & 0 & 0 & 0 & 1 \\ 1 & 1 & 1 & 1 & .... & 1 & 1 & 1 & 0 \end{bmatrix} \quad (6)$$

Using the ODP formulation presented in (11) and (5) will yield the following optimal DFR placement (ODP) for the radial transmission network of Fig. 3.

$$X^T = \begin{array}{cccccccccc} & 1 & 2 & 3 & 4 & ..... & n-3 & n-2 & n-1 & n \\ & [\mathbf{1} & 0 & 0 & 0 & ..... & \mathbf{1} & \mathbf{1} & 0 & \mathbf{1}] \end{array}$$

This implies that buses 1, $n-2$, $n-3$, and $n$ are now the optimal locations for installing DFRs for the radial transmission network of Fig. 3.

#### 2.2 Determining The Fault Distance X

It is noted that the transmission and distribution conductors used in this work are modeled using Frequency Dependent (FD) distributed line model, Marti (1982). Three-phase voltage signals registered by DFRs are transformed from phase to modal domain using the Clarke Transformation, Dommel (1996). Voltage signals in modal domain are processed to obtain five wavelet transform coefficients (WTCs) using the Discrete Wavelet Transform (DWT) and Daubechies3 (DB3) Daubechies (1992) as the mother wavelet. The WTCs at level 1 (D1) are then processed to determine the first arrival times due to their rich high-frequency content. Finally, to reduce the noise in WTCs, these signals are squared as also done in Magnago and Abur (1998).

Three DFRs are installed at buses 1, $n-3$, and $n$ by using the Optimal DFR Placement (ODP) method in the small transmission system of Fig. 1. The next step is to determine the accurate fault distance. Consider the shortest path from bus 1 to $n$ and a fault occurring at F1 along the underground cable connecting buses 3 and 4 as shown in Fig. 1. The voltage traveling waves generated by the fault at F1 will be recorded by $DFR_1$ and $DFR_n$. Applying the Discrete Wavelet Transform (DWT) to the traveling waves (TW), the squared wavelet transform coefficients $(WTC^2)$ are obtained. These are then used to extract the time of arrivals (ToA) $t_1$ and $t_n$. It can be shown that given the travel time for each line section i, $\tau_i$, it is possible to estimate the fault travel time $\tau_x$ that follows the shortest travel time route from the fault at F1 to bus 1:

$$\tau_x = \frac{1}{2}\left( t_1 - t_n + \sum_{i=1}^{k} \tau_i \right) \quad (7)$$

where:
$t_1$ and $t_n$ are the arrival times at buses 1 and $n$ respectively,
$\tau_i$ is the traveling time for line section $i$.

Note that the travel time $\tau_x$ given by (7) is derived using $DFR_1$ as the reference and will remain valid as long as the fault occurs at any point along the shortest route between buses 1 and $n$, which is the case for fault F1. However, it is equally possible to locate any fault anywhere in the rest of line sections of the meshed network by using the shortest routes formed by the other DFR pairs: $(DFR_1, DFR_{n-3})$, and $(DFR_{n-3}, DFR_n)$.

The travel time $\tau_x$ can then be used to estimate the faulted line section $s$ in the shortest route between buses 1 and $n$, which will then be used to compute the accurate fault distance. The unknown fault section $s$ can be identified by the one satisfying the following condition:

$$\tau_x \leq \sum_{i=1}^{s} \tau_i \qquad (8)$$

The first $s$ that satisfies condition (8) will reveal the faulted line section. This estimation will then be utilized in the following expression to calculate the fault distance $X$. In the case that $s = 1$, $X$ will be determined by (9). Otherwise, for $s \geq 2$, $X$ will be computed by (10).

$$X = V_s . \tau_x \qquad (9)$$

$$X = V_s \left( \tau_x - \sum_{i=1}^{s-1} \tau_i \right) + \sum_{i=1}^{s-1} d_i \qquad (10)$$

Where:
$s$ is the faulted section.
$V_s$ is the faulted section aerial mode (mode 1) TW velocity.
$d_i$ is the line length for line section $i$.
$\tau_i$ is the traveling times for line section $i$.

Note that only the faulted section TW modal speed $V_s$ is used in the estimation of $X$. Also, $\tau_i$ and $d_i$ for each line section $i$ are known parameters from network topology. Therefore, the TW modal speed differences in line-cable hybrid networks will not impact the accuracy of fault distance estimation since only one TW modal speed ($V_s$) is utilized in the computation of $X$.

### 2.3 Vectorizing Fault Location Algorithm

In order to generalize the version above and identify faults anywhere in the network, the four previous equations are put in an array as shown in 7, 8, 9, and 10. The number of DFR pairs, $q$, for a given network can be estimated by (11), where $p$ is the number of DFRs placed in the network using ODP. Therefore, there will be $q$ shortest travel time routes formed by $q$ DFR pairs that can be used to compute the arrays below.

$$q = \binom{p}{2} = \frac{(p)!}{(p-2)! \, 2!} \qquad (11)$$

The vector $\tau_k$, for $k = 1, 2, ..., q$, which stores the fault travel times $\tau_x$ for shortest travel time routes $q$ can be computed by:

$$\left[ \tau_k \right]_{q \times 1} = \frac{1}{2} \left( \left[ t_{r_k} \right]_{q \times 1} - \left[ t_{j_k} \right]_{q \times 1} + \left[ \sum_{i=1}^{u} \tau_i^{(r,j)_k} \right]_{q \times 1} \right) \qquad (12)$$

Where:
$(r, j)_k$ is the shortest route $k$, for $k = 1, 2, .., q$, between terminal buses $r$ and $j$, where $r$ is the reference bus and $j$ is the end bus.
$t_{r_k}$ is the arrival time registered at reference bus $r_k$.
$t_{j_k}$ is the arrival time registered at end bus of line $j_k$.
$\tau_i^{(r,j)_k}$ is the travel time for line section $i$ at the shortest route $(r, j)_k$.
$u$ is the number of line sections at shortest route $(r, j)_k$.

The fault travel time vector $\tau_k$ computed in (12) will be used below to identify the $q$ faulted line sections corresponding to the $q$ shortest travel time routes as follows:

$$\left[ \tau_k \right]_{q \times 1} \leq \left[ \sum_{i=1}^{s_i^{(r,j)_k}} \tau_i^{(r,j)_k} \right]_{q \times 1} \qquad (13)$$

Where:
$s_i^{(r,j)_k}$ is the faulted line section $i$ for shortest route $(r, j)_k$. These faulted sections are then stored in the array $s_k$ as shown below:

$$\left[ s_k \right]_{q \times 1} = \left[ s_i^{(r,j)_1} \quad s_i^{(r,j)_2} \quad s_i^{(r,j)_3} \quad ..... \quad s_i^{(r,j)_{(q-1)}} \quad s_i^{(r,j)_q} \right]^T \qquad (14)$$

Each element stored in vector $s_k$ is then utilized to compute the fault distance vector $X_k^{s=1}$ using (15) for all faulted line sections of $s_i^{(r,j)_k} = 1$. Otherwise, zero will be stored in vector (15).

$$\left[ X_k^{s=1} \right]_{q \times 1} = \left( \left[ V_{s_i}^{(r,j)_k} \right]_{q \times 1} \right) * \left( \left[ \tau_k \right]_{q \times 1} \right) \qquad (15)$$

For all other line sections of $s_i^{(r,j)_k} \geq 2$ in (14), the fault distance vector $X_k^{s \geq 2}$ can be estimated by (16). Otherwise, zero will be stored in vector (16).

$$\left[ X_k^{s \geq 2} \right]_{q \times 1} = \left( \left[ V_{s_i}^{(r,j)_k} \right]_{q \times 1} \right) * \left( \left[ \tau_k \right]_{q \times 1} - \left[ \sum_{i=1}^{s^{(r,j)_k}-1} \tau_i^{(r,j)_k} \right]_{q \times 1} \right) + \left[ \sum_{i=1}^{s^{(r,j)_k}-1} d_i^{(r,j)_k} \right]_{q \times 1} \qquad (16)$$

Where:
($*$) is the symbol for element-by-element multiplication of two vectors.
$V_{s_i}^{(r,j)_k}$ is the TW modal speed at faulted section $i$ for shortest route $(r, j)_k$.
$d_i^{(r,j)_k}$ is the distance for line section $i$ at the shortest route $(r, j)_k$.
The fault distance vector $X_k$ can then be determined by adding the two vectors (15) and (16) as follows:

$$\left[ X_k \right]_{q \times 1} = \left[ X_k^{s=1} \right]_{q \times 1} + \left[ X_k^{s \geq 2} \right]_{q \times 1} \qquad (17)$$

The $q \times 1$ array $X_k$ contains the fault distances computed from the reference buses of the $q$ shortest travel time routes obtained from the weighted un-directed graph $G$. Therefore, the estimated distances stored in $X_k$ will point to the same fault location in the network but observed from different reference points.

### 2.4 Determining The Accurate Fault Distance

Since the fault distances stored in $X_k$ are computed from different reference buses, it is not possible to determine the

correct fault distances and routes. However, computing the fault occurrence time vector $t_{f_k}$ corresponding for each value at $X_k$ given by (18) will lead to the correct fault distances.

$$[t_{f_k}]_{q\times 1} = [t_r]_{q\times 1} - [\tau_k]_{q\times 1} \qquad (18)$$

The fault occurrence times $t_f^{(r,j)_k}$ and fault distances $X^{(r,j)_k}$, for $k = 1, 2, ...., q$, stored in $X_k$ and $t_{f_k}$ for the $q$ shortest routes formed by $q$ DFR pairs can then form a $2D$ feature array as follows:

$$x^{(k)} = \left(t_{f_k}, X_k\right)^{(r,j)_k} \qquad (19)$$

Sorting $x^{(k)}$ in ascending order with respect to $t_f^{(r,j)_k}$ and selecting the earliest similar fault occurrence times $t_f^{(r,j)_k}$ will identify the correct fault distances $X^{(r,j)_k}$ and routes $(r,j)_k$. However, to exploit redundancy in fault distance estimation, a reference route can also be selected from the correct routes to compare the estimated distances as will be shown next.

### 2.5 Computing The Fault Distances From An Equivalent Route.

The fault distances $X^{(r,j)_k}$ stored at $x^{(k)}$ corresponding to the earliest similar fault occurrence times $t_f^{(r,j)_k}$ will lead to the identification of the correct fault locations. These distances are not comparable to each other because they are determined using different reference DFRs. However, these distances can be transformed to be comparable by selecting an equivalent route "$e$". For the case that $s_i^{(r,j)_e} = 1$, $X_e$ will be estimated by (20). Otherwise, for all the other cases when $s_i^{(r,j)_e} \geq 2$, $X_e$ will be computed by (21).

$$[X_k^e]_{q\times 1} = \left([V_{s_i}^{(r,j)_e}]_{q\times 1}\right) * \left([t_{r_e}]_{q\times 1} - [t_{f_k}]_{q\times 1}\right) \qquad (20)$$

$$[X_k^e]_{q\times 1} = \left([V_{s_i}^{(r,j)_e}]_{q\times 1}\right) * \left([t_{r_e}]_{q\times 1} - [t_{f_k}]_{q\times 1} - \left[\sum_{i=1}^{s^{(r,j)_e}-1} \tau_i^{(r,j)_e}\right]_{q\times 1}\right) + \left[\sum_{i=1}^{s^{(r,j)_e}-1} d_i^{(r,j)_e}\right]_{q\times 1} \qquad (21)$$

Note that only the vector $t_{f_k}$ contains different values in the computation of $X_k^e$ in (20) and (21). Otherwise, the entries of the other $q \times 1$ arrays will be the same due to the selection of equivalent route $e$. Therefore, a new $2D$ feature vector $x_e^{(k)}$ can be computed using the equivalent fault distances as follows:

$$x_e^{(k)} = \left(t_{f_k}, X_k\right)^{(r,j)_k} \qquad (22)$$

Sorting $x_e^{(k)}$ in descending order with respect to $X_k^e$ and extracting the largest fault distances of similar lengths

from $x_e^{(k)}$ will form the final distance vector $d$ as shown below:

$$d = [d_1 \ d_2 \ d_3 \ ........ \ d_{p-1} \ d_p] \qquad (23)$$

Where, "$p$" are the shortest paths in network containing the faulted section. In array $d$, all the fault distances must be approximately equal. Thus, taking the median will detect and eliminate outliers from the entries of $d$ vector making the fault location algorithm robust against bad data and synchronization time errors.
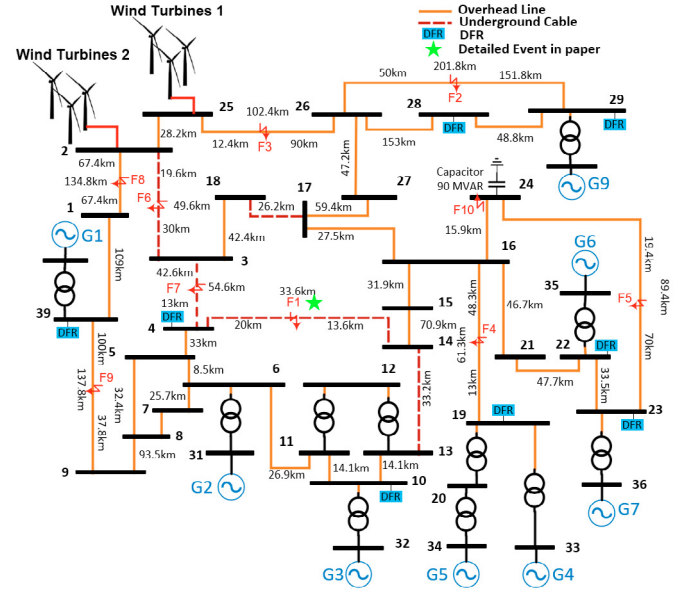


Fig. 4. IEEE 39 Bus System

## 3  Simulation Results

### 3.1  Network Model and DFR Placement

The IEEE 39 Bus System whose model data for EMT-type simulations studies developed by CIGRE (accessed February 3, 2018) is used to validate the fault location algorithm proposed in this work. Two wind generators of type-III (Doubly-fed induction Generator, DFIG), and type-IV (Full Frequency Converter, FFC), whose detailed model can be found in Karaağaç et al. (2019), are connected to buses 2 and 25. Following the procedure of Optimal DFR Placement (ODP) established in section 2.1, eight DFRs (light blue) in Fig. 4 are required to make the system identifiable for any fault in the network. Note that the transmission system is formed by overhand lines and cables as specified in Fig. 4. The traveling wave speed for overhead lines is $300,000$ Km/s and for cables is $148,130$ Km/s. Additionally, a sampling frequency of 1MHz is required to estimate accurate fault distances.

Table 1. ToA(ms) for Fault F1

| DFR | ToA$_{F1}$ | DFR | ToA$_{F1}$ |
|-----|-----------|-----|-----------|
| 4   | 30.825    | 23  | 31.476    |
| 10  | 31.053    | 39  | 31.815    |
| 19  | 31.329    | 28  | 32.192    |
| 22  | 31.440    | 29  | 32.354    |

### 3.2 Fault Location in Transmission Network

#### 3.2.1 SLG Fault at F1 13.6 km from bus 14:

A single-line-to-ground (SLG) fault F1 shown in Fig. 4 occurs along the 33.6 Km underground cable, which connects buses 4-14, 13.6 Km from bus 14. The fault is simulated using a 80 $\Omega$ fault resistance and a $30°$ fault inception angle, which is set to $30.69\ ms$. The network is then modeled as an weighted undirected graph $G$ to place 8 DFRs using ODP at the network. The fault-generated voltage signals registered by 8 DFRs are processed using discrete wavelet transform (DWT) to obtain the squared wavelet transform coefficients $(WTC^2)$ from which the time of arrivals (ToAs) are extrated as shown in Table 1. Using (11), 28 shortest travel time routes formed by 8 DFRs in graph $G$ are identified. These shortest route and ToAs are used as entries in terms (12), (13) to determine the fault travel time $\tau_k$ and fault section $s_k$ vectors. These two vectors are then used in terms (15), (16), (17) and (18) to compute the $2D$ feature vector $x^{(k)}$ as shown below:

$$x^{(k)} = \Big[ (30.69, 19.975)^{(4,23)}\ (30.69, 19.97)^{(4,19)}\ (30.69, 19.965)^{(4,22)}$$
$$(30.691, 204.94)^{(23,39)}\ (30.691, 160.95)^{(19,39)}\ (30.691, 194.05)^{(22,39)}$$
$$............\ (31.402, 11.32)^{(4,23)}\ (32.19, 19.9749)^{(4,23)} \Big]_{28 \times 1}$$

Note that the vector $x^{(k)} = (t_{f_k}, X_k)^{(r,j)_k}$ is sorted ascending with respect $t_{f_k}$ vector to make identifiable the correct fault distances in $X_k$. However, not all these distances are comparable each other. Hence these can be transformed selecting an equivalent route and using the term (20) or (21). Any of the shortest routes corresponding to the earliest fault occurrence times in $t_f$ can be selected, for instance, the shortest route $(4, 23)$ of faulted section $s = 1$ is selected for this case. Therefore, term (20) is used to compute the vector $x_e^{(k)}$, which is sorted descending with respect $X_k^e$ as shown below.

$$x_e^{(k)} = \Big[ (30.69, 19.975)^{(4,23)}\ (30.69, 19.97)^{(4,23)}\ (30.69, 19.965)^{(4,23)}$$
$$(30.691, 18.847)^{(4,23)}\ (30.691, 18.8430)^{(4,23)}\ (30.691, 18.8385)^{(4,23)}$$
$$............\ (31.402, -85.45)^{(4,23)}\ (32.19, -202.44)^{(4,23)} \Big]_{28 \times 1}$$

The negative values in $x_e^{(k)}$ mean that the fault are not located in the shortest routes formed by their DFR pairs. Finally, extracting the largest fault distances of similar lengths from $x_e^{(k)}$ will form the final distance vector $d$ as shown below:

$$d = [19.9749\ \ 19.970\ \ 19.965]$$

The median method is used to detect and remove outliers from $d$. Once the detected outliers are removed, the mean will yield the best estimate for the fault distance of 19.97 km, which will yield a error of 30 m comparing the the actual distance of 20 km.

### 3.3 Simulated Cases With Different Fault Parameters

Faults are simulated using the IEEE 39-bus system in Fig. 4 by using different fault parameters such as the fault resistance and inception angle, in the presence of non-transposed lines and having IBPSs in the transmission network. Simulation results yield maximum and average absolute errors of 35.78 m and 18.18 m respectively as shown in Table 2. These results provide experimental evidence that the network configuration and fault types do not have significant impact on the performance of the proposed algorithm.

Table 2: Fault Location Errors at IEEE 39 Bus System.

| Fault | Location | Rf | Fault Angle | Fault Type | Err (m) |
|---|---|---|---|---|---|
| F2 | 24.77% $L_{26-29}$ | 40$\Omega$ | 135° | B-g | 17.25 |
| F3 | 12.10% $L_{25-26}$ | 80$\Omega$ | 70° | A-g | 32.5 |
| F4 | 21.20% $L_{19-16}$ | 20$\Omega$ | 90° | C-g | 25.4 |
| F5 | 21.70% $L_{24-23}$ | 40$\Omega$ | 60° | BC-g | 12.5 |
| F6 | 39.51% $L_{2-3}$ | 30$\Omega$ | 45° | ABC-g | 8.5 |
| F7 | 23.80% $L_{4-3}$ | 50$\Omega$ | 120° | ABC | 7.25 |
| F8 | 50.00% $L_{1-2}$ | 60$\Omega$ | 10° | B-g | 35.78 |
| F9 | 27.43% $L_{9-39}$ | 100$\Omega$ | 30° | AC-g | 15.7 |
| F10 | BUS24 | 140$\Omega$ | 75° | AB | 8.75 |

### 4 Conclusion

This paper presents and validates a fast, accurate and robust fault location algorithm that can be used for any type of power network configuration. The method uses several arrays that are processed by the algorithm resulting in a straightforward calculation without the need to first identify the faulted section to determine the fault location. Despite the reduction in the calculation steps compared to authors' earlier work, the main advantages such as the robustness against gross errors in measurements, insensitivity to presence of IBPSs, and capability to differentiate faults from other events are all maintained in the proposed algorithm. The IEEE 39-bus system is used to validate the proposed algorithm performance under different fault types and conditions using extensive simulations.

### References

CIGRE (accessed February 3, 2018). *Power system test cases for EMT-type simulation studies.* https://e-cigre.org/publication/736-power-system-test-cases-for-emt-type\\-simulation-studies.

Daubechies, I. (1992). *Ten lectures on wavelets*, volume 61. Siam.

Ding, J., Wang, X., Zheng, Y., and Li, L. (2018). Distributed traveling-wave-based fault-location algorithm embedded in multiterminal transmission lines. *IEEE Transactions on Power Delivery*, 33(6), 3045–3054.

Dommel, H.W. (1996). *EMTP theory book*. Microtran Power System Analysis Corporation.

Filomena, A.D., Salim, R.H., Resener, M., and Bretas, A.S. (2008). Ground distance relaying with fault-resistance compensation for unbalanced systems. *IEEE Transactions on Power Delivery*, 23(3), 1319–1326. doi:10.1109/TPWRD.2007.909210.

Galvez, C. and Abur, A. (2020). Fault location in active distribution networks containing distributed energy resources (DERs). *IEEE Transactions on Power Delivery*, 1–1. doi:10.1109/TPWRD.2020.3034179.

Galvez, C. and Abur, A. (2022). Fault location in power networks using a sparse set of digital fault recorders. *IEEE Transactions on Smart Grid*, 13(5), 3468–3480.

doi:10.1109/TSG.2022.3168904.

Karaağaç, U., Mahseredjian, J., Gagnon, R., Gras, H., Saad, H., Cai, L., Koçar, I., Haddadi, A., Farantatos, E., Bu, S., Chan, K.W., and Wang, L. (2019). A generic emt-type model for wind parks with permanent magnet synchronous generator full size converter wind turbines. *IEEE Power and Energy Technology Systems Journal*, 6(3), 131–141.

Magnago, F. and Abur, A. (1998). Fault location using wavelets. *IEEE Transactions on Power Delivery*, 13(4), 1475–1480. doi:10.1109/61.714808.

Marti, J.R. (1982). Accurate modeling of frequency-dependent transmission lines in electromagnetic transient simulations. *IEEE Power Engineering Review*, PER-2(1), 29–30. doi:10.1109/MPER.1982.5519686.

Paladhi, S. and Pradhan, A.K. (2020). Adaptive distance protection for lines connecting converter-interfaced renewable plants. *IEEE Journal of Emerging and Selected Topics in Power Electronics*, 1–1. doi:10.1109/JESTPE.2020.3000276.

Sachdev, M.S. and Agarwal, R. (1988). A technique for estimating transmission line fault locations from digital impedance relay measurements. *IEEE Transactions on Power Delivery*, 3(1), 121–129. doi:10.1109/61.4237.

SEL ((accessed 2022)). *Time-Domain Line Protection*. https://selinc.com/products/T400L.

Yadav, A. and Swetapadma, A. (2015). Enhancing the performance of transmission line directional relaying, fault classification and fault location schemes using fuzzy inference system. *IET Generation, Transmission Distribution*, 9(6), 580–591. doi:10.1049/iet-gtd.2014.0498.